

OPEN ACCESS

Microstructures in laser welded high strength steels

To cite this article: P Rizzi *et al* 2009 *J. Phys.: Conf. Ser.* **144** 012005

View the [article online](#) for updates and enhancements.

You may also like

- [Laser welding of AISI 410S ferritic stainless steel](#)
Ceyhun Köse and Ceyhun Topal
- [Effect of laser welding and laser wire filling on forming and properties of dissimilar steel welded joints](#)
Sun Lina, Lu You and Jiang Junxiang
- [Recent advances in mitigating fusion zone softening during laser welding of Al-Si coated 22MnB5 press-hardened steels](#)
Muhammad Shehryar Khan



ECS
The
Electrochemical
Society
Advancing solid state &
electrochemical science & technology

DISCOVER
how sustainability
intersects with
electrochemistry & solid
state science research

Microstructures in laser welded high strength steels

P Rizzi^{1,3}, S Bellingeri², F. Massimino¹, D Baldissin¹, L Battezzati¹

¹Dip. Chimica IFM and NIS, Università di Torino, V. Giuria 7, 10125 Torino, Italy

²Elasis S.C.p.A. - Product & Process Development, V. Bistagno 10, 10136 Torino, Italy

³paola.rizzi@unito.it

Abstract. In this work, the effect of laser welding on the microstructure was studied for three Advanced High Strength Steels: transformation induced plasticity steel (TRIP), dual phase steel (DP) and martensitic steel. Two sheets of the same steel were laser welded and a microstructural study was performed by optical microscopy, scanning electron microscopy and X-ray diffraction. For all samples the welded zone was constituted by martensite and the heat affected zone shows a continuous change in microstructure depending on temperatures reached and on the different cooling rates. The change in mechanical properties in the welded area was followed by Vickers micro-hardness measurements. Quasi binary phase diagrams were calculated and, according to position of T_0 lines, it was deduced that austenite is the primary phase forming during rapid solidification for all steels.

1. Introduction

The stringent demands for safety increase and weight reduction in the automotive industry have driven the development of advanced high strength steels (AHSS), having good combination of ductility and strength [1, 2]. With these, thinner sheets can possibly be used in automobile bodies since AHSS have better impact energy absorbing capacity and resistance to plastic deformation with respect to conventional ferritic low-carbon sheet steels. AHSS include dual phase (DP), transformation induced plasticity (TRIP), complex phase (CP) and martensitic (M) steels, all displaying yield strength higher than 300 MPa and tensile strength higher than 600 MPa [3, 4].

In parallel with the evolution of AHSS, the laser welding process has received attention because of high-production rate and good metallurgical properties of the joined metals: reduced extension of the heat affected zone (HAZ) and welded zone (WZ), and lower residual stresses [5, 6]. Therefore, it is of great interest to monitor the microstructure of the AHSS after laser welding to keep the resistance to plastic deformation and impact energy absorbing capacity, i.e. the passive automobile safety.

Laser welding implies rapid heating of a limited volume of alloy which is molten and rapidly re-solidified via heat extraction from the cold material in contact with it. Analysing the microstructure of the WZ and HAZ provides information on the solidification mechanism for improved process control.

In this work, three automotive AHSS (DP, M and TRIP) are studied in order to reveal the solidification mechanism the change in microstructure and mechanical properties following laser welding. The TRIP steel will be extensively described and compared with the results obtained for the other materials.

2. Experimental

The composition of the steels used in this work is (all values in weight %): TRIP: C = 0.213%, Si = 1.76%, Mn = 1.64%, Al = 0.041%, P = 0.013%, (Ni+Cr+Mo) = 0.051%, Cu = 0.021%, traces of V, S, Nb, Ti, B; DP: C = 0.161%, Si = 0.41%, Mn = 1.79%, Al = 0.045%, P = 0.013%, S = 0.007%, B = 0.0015%; M: C = 0.227%, Si = 0.23%, Mn = 1.12%, Al = 0.037%, Ti = 0.029%, P = 0.013%.

Laser welding experiments were performed with a Nd YAG Laser with power of 3.8 kW and focalised spot of 0.64 mm. Two sheets of the same steel were joined by using welding rates of 0.8 m/min, 1 m/min, 2 m/min for DP, M and TRIP steel respectively. Thickness of sheets were 2.1 mm for DP and M and of 1.5 mm for TRIP. Full penetration was obtained in all samples.

Metallographic observations were done by both optical (OM) and scanning electron (SEM) microscopy with Nital 3% etching. A Vickers tester was used for microhardness measurements with a load of 500 gf, along a line through the centre of the sheet encompassing the HAZ and the WZ.

3. Results and discussion

3.1. Phase diagrams

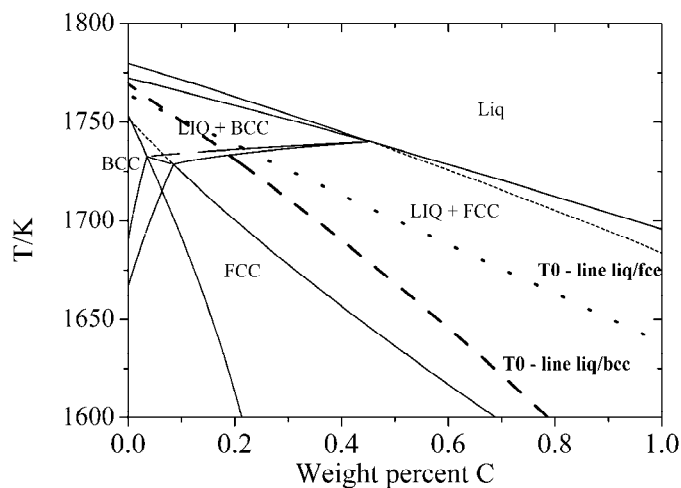


Figure 1. TRIP quasi binary phase diagram.

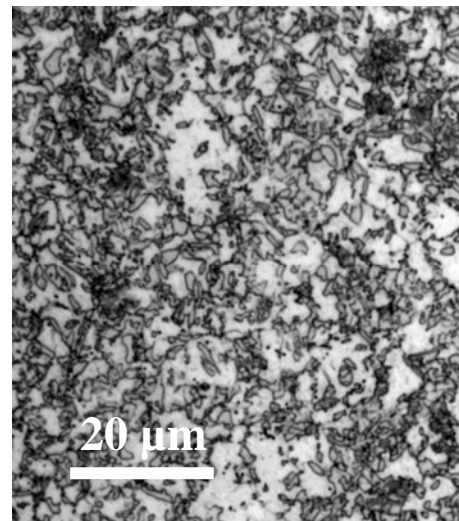


Figure 2. MO micrograph of untransformed TRIP

The quasi binary phase diagrams of the three steels were calculated by using the Thermocalc software [6]. As an example, the result for TRIP steel is reported in Fig 1 by fixing the Si and Mn content at 1.76 % wt. and 1.64 % wt., respectively, together with the T₀ lines for δ-ferrite (bcc) and austenite (fcc). For the present C content in the steel, the formation of δ-ferrite is expected in equilibrium conditions. However, the laser welding process implies rapid quenching of the melt with the possible occurrence of substantial undercooling. The T₀ lines for the bcc and fcc phases are very close to each other and intersect at 0.09 %wt. C. So, for low C content, the T₀ line for ferrite is encountered at higher temperature and formation of δ-ferrite is favoured even on undercooling; for C content higher than 0.09 %wt, the line sequence is reversed and the formation of austenite is expected when the system deviates from the equilibrium conditions.

3.2. Microstructures and microhardness

The untransformed TRIP steel is constituted by ferrite, bainite and austenite (fig 2). When laser welding is performed, a change in microstructure is observed in the WZ with formation of martensite (fig 3). The thickness of the WZ is limited to about 1.7 mm. The HAZ contains three phases: ferrite, austenite and martensite (or bainite). The amount of these phases continuously changes from the base metal to the WZ, because of the combined differences in cooling rates and temperatures reached during welding. Near the

WZ, where higher temperatures are reached and high cooling rates can be inferred, a large amount of martensite is found beside a small amount of austenite and ferrite (fig. 4). On the contrary, near the base metal a large amount of austenite is found beside ferrite and bainite; martensite cannot be formed because of the low cooling rates acting during cooling in this zone of the sample.

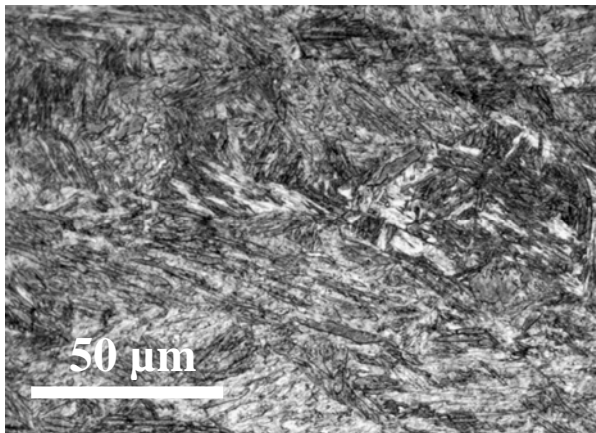


Figure 3. MO micrograph of WZ of TRIP

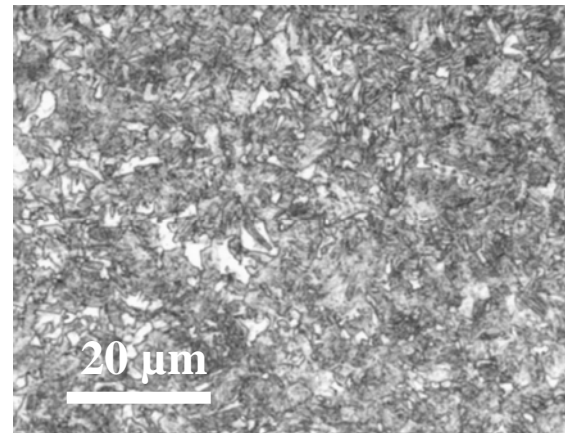


Figure 4. MO micrograph of HAZ of TRIP

The microhardness of the different zones is consistent with the interpretation of the microstructure, having values of 278 ± 6 Hv in the untransformed zone and 543 ± 24 Hv in the WZ. In the HAZ an increasing value is measured, raising from the hardness of the base metal to that of the WZ, as shown in fig 5 where the hardness vs. distance from the WZ is reported. This is due to different amounts of ferrite, austenite and martensite (or bainite) present in such zone dependent on the distance from the WZ.

As discussed above, the primary formation of austenite is expected in TRIP when enough undercooling is reached. In the WZ columnar growth of the austenite during solidification [7] can be inferred because of the presence of the ghost microstructure of the primary grains, still visible after transformation to martensite. Apparently, the austenite grows from the HAZ grains towards the centre of the liquid pool following the trend of the temperature gradient. Should primary ferrite having been formed, austenite would have been produced via a solid state transformation. Because of the fast cooling, however, either the

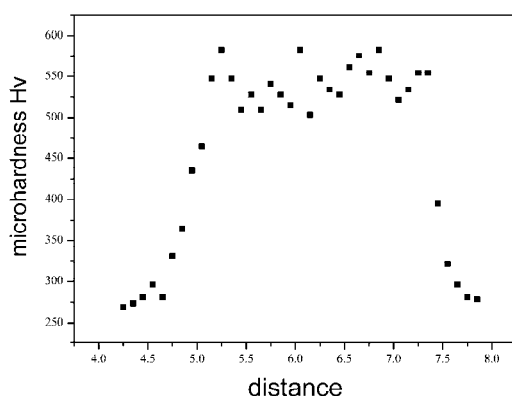


Figure 5. Vickers micro hardness vs. distance from the WZ for TRIP

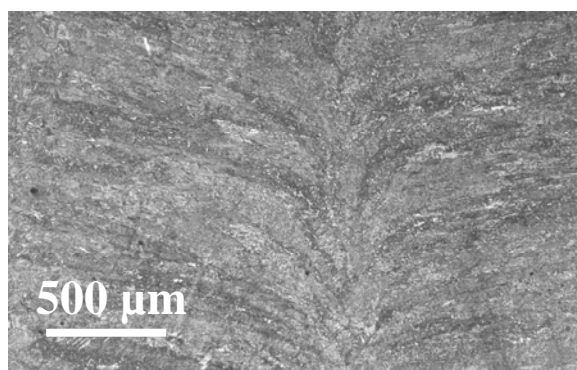


Figure 6. MO micrograph of the ghost microstructure of the primary austenite grains for DP steel.

ferrite could have been trapped below the eutectoid temperature with no formation of martensite, or it could have remained amid austenite grains as a retained skeleton [8]. Both transformation paths are not supported by the microstructural observation. The solidification of austenite as primary phase is further supported by

noting that in this study the steels were welded employing different laser speeds, as suggested by previous practice. With high energy input (DP steel) the ghost columns originating from growth (Fig. 6) are even more apparent than those observed for TRIP. Therefore, it is concluded that the undercooling within the molten pools in these steels must be high in all practical conditions of laser welding and austenite solidifies directly from the melt in partitionless fashion. This will avoid the risk of generating hot tearing cracks [9] due to the ferrite to austenite transformation in case ferrite would have solidified first. Shrinkage pores of small size were found in the WZ with a random distribution.

In short, a description of the microstructure and microhardness of the other two steels is reported. The martensitic steel is composed by martensite and a limited amount of ferrite. A similar microstructure is observed in the welded zone, giving rise to similar microhardness values (488 ± 31 Hv in the base metal and 506 ± 21 Hv in the WZ). The HAZ has different amounts of martensite, austenite and bainite passing from WZ to the base metal, due to the varied temperatures reached and quenching rates. This produces a decrease in the hardness to the lower value of 298 ± 9 Hv near the WZ.

The DP steel is constituted by a fine grained matrix of ferrite containing a uniform distribution of fine martensite islands; its hardness is 355 ± 14 Hv. Welding produces a matrix of martensite with dispersed ferrite. This microstructure causes an increase in the hardness to 453 ± 12 Hv. In the HAZ, a continuous change in microstructure is observed with the presence of ferrite, austenite and martensite (or bainite) and the hardness increases from the value of the base metal to that of the WZ.

The changes in hardness after welding are expected to reflect a corresponding change in the yield and ultimate tensile strengths. In all cases, the estimated strengths (of the order of three times the hardness) fall in the range of high strength steels. For the martensitic steel, hardness variation is limited in the WZ with respect to the base metal; the HAZ only shows a decrease of hardness related to the presence of austenite and bainite. Such microstructure, however, would imply an increase in toughness. Both DP and TRIP show an increment in hardness in the HAZ and in the WZ, especially for the TRIP.

4. Conclusions

Laser welding of DP, M and TRIP steels was performed with the aim of revealing the solidification mechanism via microstructural observation and of evaluating the mechanical properties. For all samples the WZ is constituted by martensite, due to the high cooling rates operative during solidification. Along the HAZ a continuous change in microstructure is found due to the varied temperatures reached after welding and consequent cooling rates with corresponding variations in microhardness. For TRIP, a large increment is found in the WZ (543 ± 24 Hv) with respect to the untransformed zone (278 ± 6 Hv). For the M steel, the hardness in the WZ is close to that of the base metal and the HAZ only shows a decrease related to the presence of austenite and bainite. For all steels, the formation of austenite as primary phase is expected due to solidification undercooling.

5. Acknowledgments

Work partially performed in the framework of the ESA-Thermolab project "High-Precision Thermophysical Property Data of Liquid Metals for Modelling of Industrial Solidification Processes".

References

- [1] Li Y., Lin Z., Jiang A. and Chen G. 2003 *Mater. Design* **24** 177
- [2] Merklein M and Lechler J. 2006 *J. Mater. Process. Tech.* **177** 452
- [3] De Cooman B.C., 2004 *Curr. Opin. Solid St. M.* **8** 285
- [4] Zhang M., Li L., Fu R.Y., Krizan D. and De Cooman B.C. 2006 *Mat. Sci. Eng. A* **438–440** 296
- [5] Xia M., Tian Z., Zhao L. and Zhou Y.N. 2008 *Mater. Trans.* **4** 746
- [6] Thermocalc is a software product of Thermo-Calc AB, Stockholm, Sweden.
- [7] David S.A., Babu S.S., and Vitek J.M. 2003 *JOM* **6** 14
- [8] Baldissin D., Baricco M., Battezzati L. 2007 *Mat. Sci. Eng. A* **449–451** 999
- [9] Hatami N., Babaei R., Dadashzadeh M., Davami P. 2008 *J Mater Process Tech* **205** 506